Simulating the Double-slit Experiment Using the Crank-Nicolson Method

Sophus B. Gullbekk, Erlend Kristensen, Tov Tyvold, Jonathan Larsen
(Dated: December 15, 2021)

The double-slit experiment is used to study the behavior of a single non-relativistic particle. To simulate this experiment, we start by removing all dimensions from the Schrödinger equation. We then discretize the equation according to the Crank-Nicolson approach. We initialize the simulation with a Gaussian wave packet and a potential barrier given by the matrix V. The potential barrier can represent three different slit configurations. We use the Born rule to transform the Scrödinger equation to a probability function and visualize the change in the probability over time. Lastly, we measure the particle using a detector screen at $x = 0.8$ and make a plot of the detection probability. The single-slit configuration shows a Gaussian distribution, while both the double- and triple-slit configurations show an interference pattern.

I. INTRODUCTION

The *double-slit experiment* is a famous experiment known for illustrating some of the central mysteries in quantum mechanics. It demonstrates the *wave-particle duality* of quantum objects, which tells us that they can behave both as a particle and a wave. The experiment was first demonstrated by *Thomas Young* in 1801. He shone a light through two slits and observed an interference pattern [1]. We will simulate a version of Young's experiment and use it to demonstrate the behaviour of a single non-relativistic particle. More precisely, we want to show the interference pattern that emerges when the wave particle interacts with the barrier-slits.

At the core of our simulation is the time-dependent *Schrödinger equation*. It is a partial differential equation, where the solution gives us the complex valued *wave function* $\Psi(x, y, t)$. This solution is linked to probability through the *Born rule*, which tells us that $|\Psi|^2$ gives us the probability density that we will find a particle at a certain position inside the room. Therefore, to perform a simulation of the double-slit experiment we need to solve the time-dependent Schrödinger equation and convert it to a probability density function.

To solve a partial differential equation numerically, we use a finite difference method. The method is called *Crank-Nicolson* and it is well suited to solve partial differential equations similar to the Schrödinger equation. The Crank-Nicolson method is time-dependent, implicit, stable and gives rise to a sparse matrix equation that can be solved efficiently using the *LU decomposition*. The properties of the Crank-Nicolson method makes it a good choice for simulation the experiment.

In section II we introduce the relevant theory and the methods used in our implementation. In section III we represent the results of the simulations. We then move on to discussing the results in section IV. Finally, we summarize our findings in section V.

II. THEORY AND METHODS

A. Wave Mechanics

In 1926 Erwin Schrödinger went on a Christmas vacation with a mistress to a cabin deep into the Swiss Alps. When he returned early the following year, he brought with him the famous Schrödinger equation. He had discovered wave mechanics [2].

A quantum object has both particle-like and wave-like properties and is therefore much more complex than a classical Newtonian particle. A quantum object can be viewed as spread out over a region of space, which we will refer to as a *probability cloud*. The quantum object will follow a behaviour governed by the Schrödinger equation. The general formulation of the time-dependent Schrödinger equation is

$$i\hbar\frac{d}{dt}|\Psi\rangle = \hat{H}|\Psi\rangle,$$

where $\hat{H}$ is the *Hamiltonian* operator, $\hbar$ is the *reduced Planck constant* and $|\Psi\rangle$ represents the *quantum state*. We will consider the case of a single non-relativistic particle in two dimensional "position space". We can then view $|\Psi\rangle$ as the complex valued wave function $\Psi(x, y, t)$. This transforms the Schrödinger equation into

$$i\hbar\frac{\partial}{\partial t}\Psi(x,y,t) = -\frac{\hbar^2}{m}\left(\frac{\partial^2}{\partial x^2} + \frac{\partial^2}{\partial y^2}\right)\Psi(x,y,t) + V(x,y,t)\Psi(x,y,t).$$

Here, m represents the mass of the particle. The first two terms describes the kinetic energy and the last term represents the potential energy. V is a potential that describes the external environment of the experiment, in our simulations it will be a time-independent value so that $V(x, y, t) = V(x, y)$.

The quantum state described by Schrödinger's equation is related to probability through the Born rule. It acts as a bridge between the mathematical formalism of quantium theory and experiment [3]. For our system so far, the Born rule takes the form:

$$p(x,y;t) = |\Psi(x,y,t)|^2 = \Psi^*(x,y,t)\Psi(x,y,t),$$

where, $p(x,y;t)$ is the probability density for detecting the particle at position (x,y) if we measure it at time t.

B. The Dimensionless Schrödinger Equation

In our simulations we will keep things simple by using dimensionless variables. This leaves us with a "bare" Schrödinger equation:

$$i\frac{\partial u}{\partial t} = -\frac{\partial^2 u}{\partial x^2} - \frac{\partial^2 u}{\partial y^2} + v(x,y)u. \tag{1}$$

Here, $u(x,y,t)$ is the wave function and $v(x,y)$ is the potential.

With the new version of the Schrödinger equation, the Born rule takes the form

$$p(x,y;t) = |u(x,y,t)|^2 = u^*(x,y,t)\cdot u(x,y,t). \tag{2}$$

We assume that the function $u(x,y,t)$ is properly normalized.

C. Crank-Nicolson

The Schrödinger equation given in equation 1 is a partial differential equation (PDE). We want to use the Crank-Nicolson method to numerically solve the PDE and find the evolution of $u(x,y,t)$ as it interacts with the potential $v(x,y)$.

The Crank-Nicolson method can be derived from two well known finite difference methods. The explicit forward difference scheme is given as

$$\frac{u_{i,j}^{n+1} - u_{i,j}^n}{\Delta t} = F_{i,j}^n. \tag{3}$$

The implicit backwards difference scheme is given as

$$\frac{u_{i,j}^{n+1} - u_{i,j}^n}{\Delta t} = F_{i,j}^{n+1}. \tag{4}$$

In both cases i,j are spatial indices and the superscript n is the time index. The Crank-Nicolson method is simply a linear combination of equations 3 and 4 with 1/2 as scalar coefficients:

$$\frac{u_{i,j}^{n+1} - u_{i,j}^n}{\Delta t} = F_{i,j}^{n+1} + F_{i,j}^n. \tag{5}$$

This method is implicit, of second order and numerically stable - making it suitable to solve our PDE.

Using the discretizations given in the equations B1 and B2 found in appendix B with the method from equation 5, we get the full discretized form of equation 1:

$$\begin{aligned} u_{i,j}^{n+1} &- r\left[u_{i+1,j}^{n+1} - 2u_{i,j}^{n+1} + u_{i-1,j}^{n+1}\right] \\ &- r\left[u_{i,j+1}^{n+1} - 2u_{i,j}^{n+1} + u_{i,j-1}^{n+1}\right] + \frac{i\Delta t}{2} v_{i,j} u_{i,j}^{n+1} \\ = u_{i,j}^{n} &+ r\left[u_{i+1,j}^{n} - 2u_{i,j}^{n} + u_{i-1,j}^{n}\right] \\ &+ r\left[u_{i,j+1}^{n} - 2u_{i,j}^{n} + u_{i,j-1}^{n}\right] - \frac{i\Delta t}{2} v_{i,j} u_{i,j}^{n}, \end{aligned} \tag{6}$$

where $r \equiv i\Delta t/2h^2$. The notation used for the discretization can be found in appendix A.

Equation 6 is a system of linear equations, which we transform into the following matrix equation:

$$A\vec{u}^{\,n+1} = B\vec{u}^{\,n}. \tag{7}$$

The vector $\vec{u}^{\,n}$ has length $(M-2)^2$. The matrices A and B are therefore of size $(M-2)^2 \times (M-2)^2$. They will have a characteristic structure due to the Crank-Nicholson approach. As an example, we show A and B for $M = 5$ in equations B7 and B8 found in appendix B. Using equation 6 we find that the main diagonal of A and B can be filled according to the following patterns:

$$a_k = 1 + 4r + \frac{i\Delta t}{2} v_{i,j}, \tag{8}$$

$$b_k = 1 - 4r - \frac{i\Delta t}{2} v_{i,j}, \tag{9}$$

where a_k and b_k is the k-th element along the main diagonal of A and B respectively.

D. Initial State

When setting up the initial state $u_{i,j}^0$, we base it on an unnormalised *Gaussian wave packet*, given as:

$$u(x,y,0) = e^{-\frac{(x-x_c)^2}{2\sigma_x^2} - \frac{(y-y_c)^2}{2\sigma_y^2} + ip_x(x-x_c) + ip_y(y-y_c)}. \tag{10}$$

Here, x_c and y_c are the coordinates of the centre of the initial wave packet, σ_x and σ_y are the initial widths of the wave packet in the x and y directions, and lastly p_x and p_y are the wave packet momenta.

After setting up the initial state $u_{i,j}^0$, we normalize it such that

$$\sum_{i,j} u_{i,j}^{0*} u_{i,j}^0 = 1. \tag{11}$$

This is to ensure that we can interpret $p_{i,j}^n = u_{i,j}^{n*} \cdot u_{i,j}^n$ as a probability and not a probability density. In other words, $p_{i,j}^n$ is the probability that the particle is located in small grid cell of area h^2 located at (x_i, y_i) at the time step n.

We have assumed *Dirichlet* boundary conditions in the xy-plane, given in equation B3 found in appendix B.

E. Implementation of the experiment

Naturally, we simulate the double-slit experiment with a double-slit configuration. The exact properties of the double-slit barrier can be adjusted using the following parameters:

- Wall thickness in x direction
- Wall position center in the x direction
- Length of the wall piece separating the two slits (the y distance between the inner edges of the two slits)
- Slit aperture (opening in the y direction)

An example of a double-slit configuration used in our simulations is shown in figure 1.

As explained earlier, we represent the barrier by a potential $v(x, y)$. We want v to be able to represent single- and triple-slit configurations as well. Therefore we have implemented similar functions for all three configurations. In total we will look at four different barrier configurations: The single-, double- and triple-slit configurations as well as turning the barrier completely off.

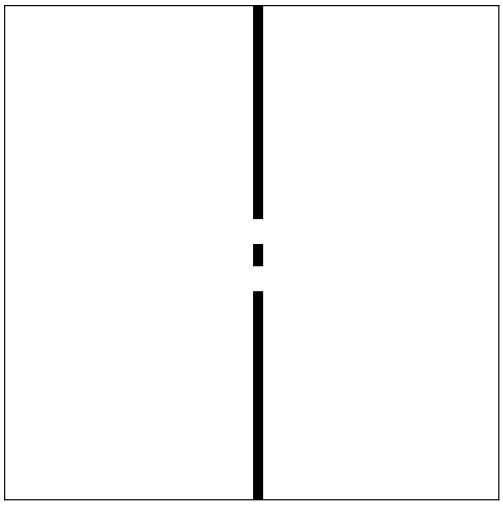

FIG. 1. This is a visualization of the double-slit barrier represented by $v(x, y)$ that is used in our simulation. The room is without units, because we are using a unitless version of the Schrödinger equation and have normalized the axes such that $x, y \in [0, 1]$.

Now that the external environment of our experiment is well defined, we can start solving equation 1 over time. This means that we have to solve the matrix equation 7, which gives us the next state $\vec{u}^{n+1}$ given by the current state $\vec{u}^{n}$. There are many different methods that we can use to solve the matrix equation. In our simulations we choose to use LU decomposition. This is a method that decomposes the matrix A into an upper and a lower triangular matrix. For our case, this is especially efficient because A is a sparse matrix with a structure that is similar to a tridiagonal matrix. The `superlu` solver is found in the armadillo library for C++ and efficiently solves a sparse system of linear equations[4] using LU decomposition.

III. RESULTS

All figures are generated using $M = 201$, making the resolution of the simulations (199×199).

Figure 2 shows the deviation of the total probability $p^n_{i,j}$ from 1.0 as a function of time between $t \in [0, 0.008]$, with and without a double-slit barrier. Figure 3 shows the probability $p^n_{i,j}$, the real part $\mathrm{Re}(u^n_{i,j})$ and the imaginary part $\mathrm{Im}(u^n_{i,j})$ when using a double-slit barrier. Each column represents one of three different time steps, $t = 0$, $t = 0.001$ and $t = 0.002$. Figure 4 shows the time evolution of the experiment for a single-slit, double-slit and triple-slit barrier over the time steps $t = 0$, $t = 0.001$ and $t = 0.002$. Finally, we have figure 5, which shows the detection probability $p(y|x = 0.8, t = 0.002)$ for same three slit configurations. This is visualized using line plots with corresponding heat maps.

All the plots that represent the room of the experiment, namely those in figure 3 and figure 4, have the axes removed. This is because we are dealing with a system without units and the scale of the room is normalized such that $x, y \in [0, 1]$.

A. Animations

We animate three different slit configurations here. They show the simulation using single-slit, double-slit and triple-slit configurations over time from $t = 0$ to $t = 0.015$. The settings used for all three animations are $h = 0.005$, $\Delta t = 2.5 \cdot 10^{-5}$, $T = 0.002$, $x_c = 0.25$, $\sigma_x = 0.05$, $p_x = 200$, $y_c = 0.5$, $\sigma_y = 0.05$, $p_y = 0$ and $v_0 = 1 \cdot 10^{10}$. All three configurations use a wall thickness of 0.02, positioned at $x = 0.5$ and with slit apertures of 0.05. The distance between the slits of the double and triple-slit configuration is of length $y = 0.05$. Instead of animating the probability $p^n_{i,j}$ given by the Born rule, we use $\sqrt{p^n_{i,j}}$ as the color value. This is done to bring forth structure in the regions of low probability.

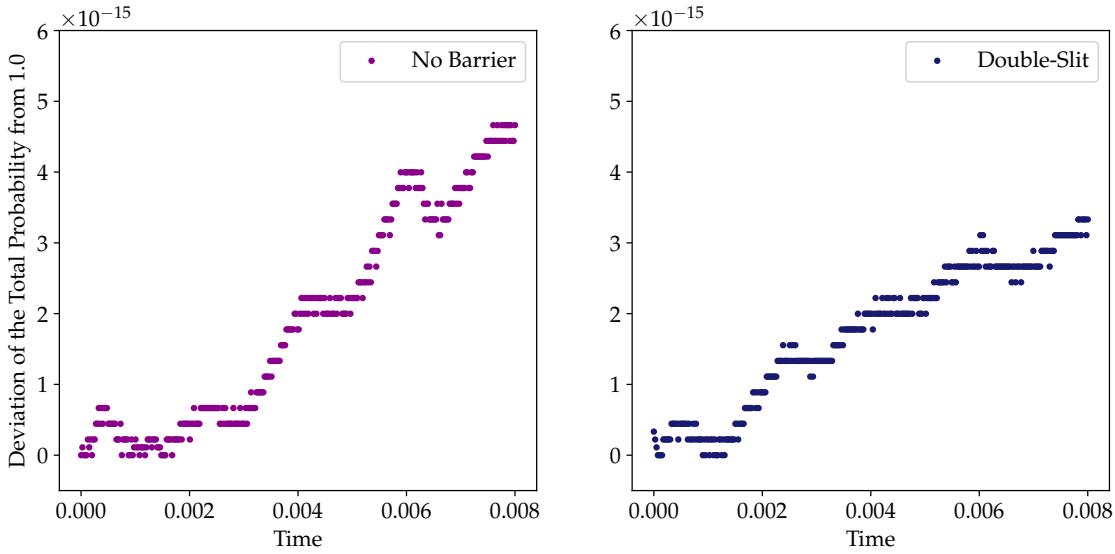

FIG. 2. A figure showing the deviation of the total probability $p^n_{i,j}$ from 1.0 as a function of time between $t = 0.0$ and $t = 0.008$. The left plot uses a setup with no barrier, while the right plot uses a barrier with a double-slit configuration. Both simulations are computed with the parameters $h = 0.005$, $\Delta t = 2.5 \cdot 10^{-5}$, $x_c = 0.25$, $\sigma_x = 0.05$, $p_x = 200$, and $p_y = 0$. The first plot has a narrower initial state in the y-direction using $\sigma_y = 0.05$ while the second uses $\sigma_y = 0.1$. The double-slit plot has a wall thickness of 0.02, positioned at $x = 0.5$ and with slit apertures of 0.05 separated by a 0.05 long piece. The potential used for the barrier is $v_0 = 1 \cdot 10^{10}$.

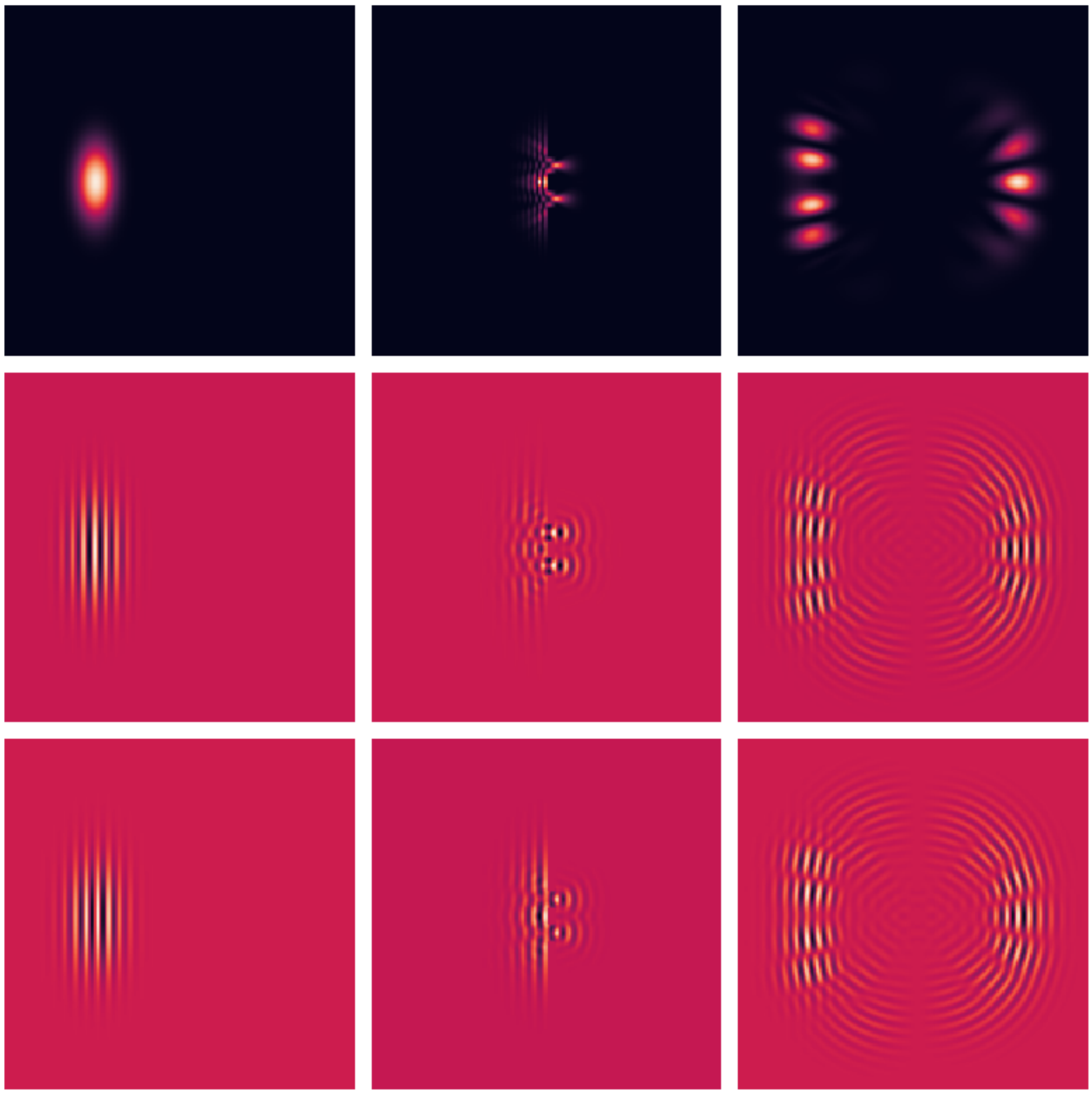

FIG. 3. A figure with three rows representing the probability $p^n_{i,j}$, the real part $\mathrm{Re}(u_{i,j})$ and the imaginary part $\mathrm{Im}(u_{i,j})$ respectively. Each column represent time step $t = 0$, $t = 0.001$ and $t = 0.002$ respectively. The parameters used for all three heat maps are $h = 0.005$, $\Delta t = 2.5 \cdot 10^{-5}$, $T = 0.002$, $x_c = 0.25$, $\sigma_x = 0.05$, $p_x = 200$, $y_c = 0.5$, $\sigma_y = 0.20$, $p_y = 0$ and $v_0 = 1 \cdot 10^{10}$. The double-slit is configured with wall thickness in x direction of 0.02, positioned at $x = 0.5$ and with slit apertures in y direction of 0.05 separated by a 0.05 long piece.

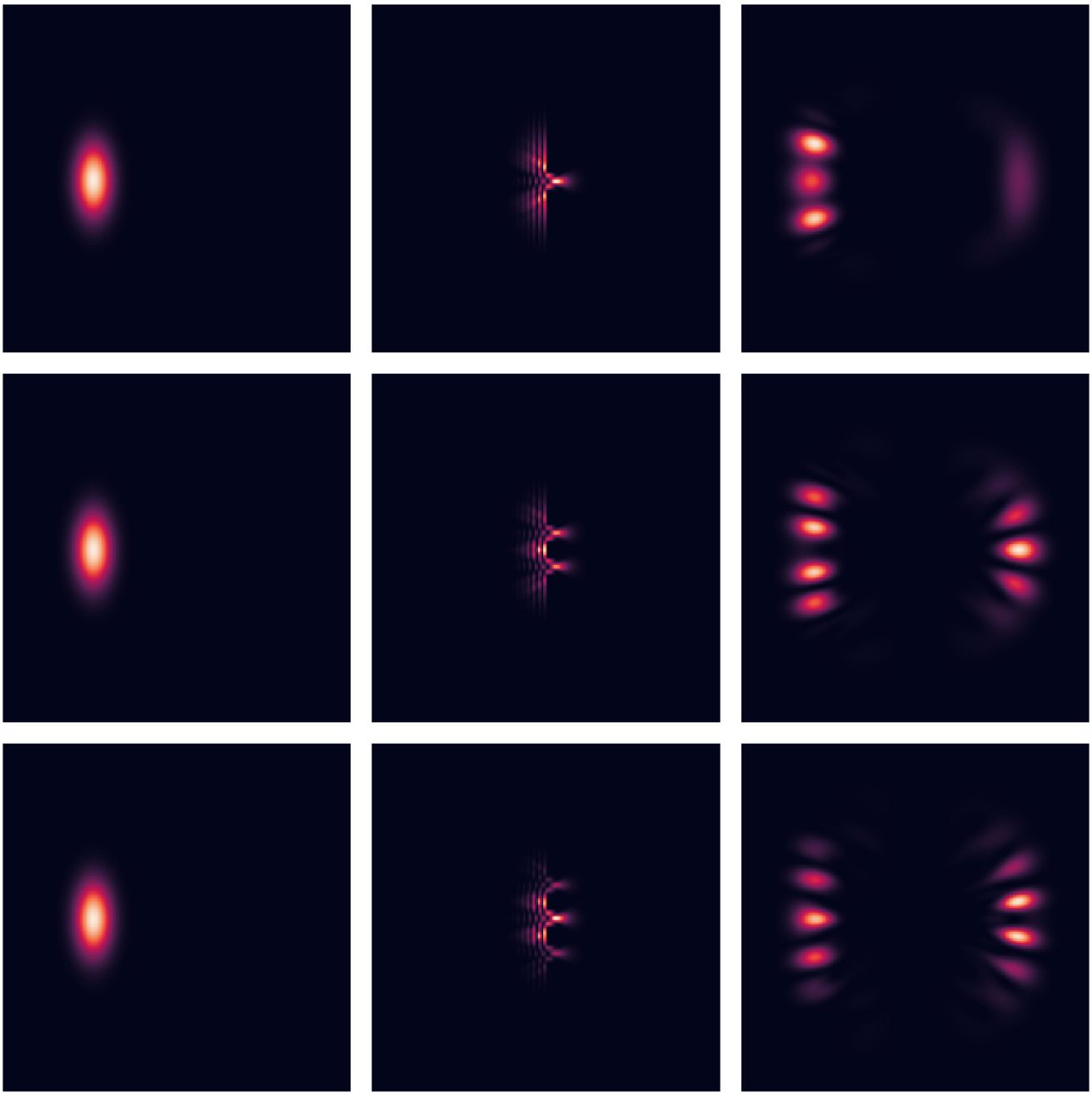

FIG. 4. A figure with three columns showing the time evolution of the experiment for three distinct times $t_0 = 0$, $t_1 = 0.001$ and $t_3 = 0.002$ respectively. The top row shows a single-slit experiment, the second row shows a double-slit experiment and the third row shows a triple-slit experiment. The parameters used for all three heat maps are $h = 0.005$, $\Delta t = 2.5 \cdot 10^{-5}$, $T = 0.002$, $x_c = 0.25$, $\sigma_x = 0.05$, $p_x = 200$, $y_c = 0.5$, $\sigma_y = 0.05$, $p_y = 0$ and $v_0 = 1 \cdot 10^{10}$. All three configurations use a wall thickness of 0.02, positioned at $x = 0.5$ and with slit apertures of 0.05. The distance between the slits of the double and triple-slit configuration is of length $y = 0.05$

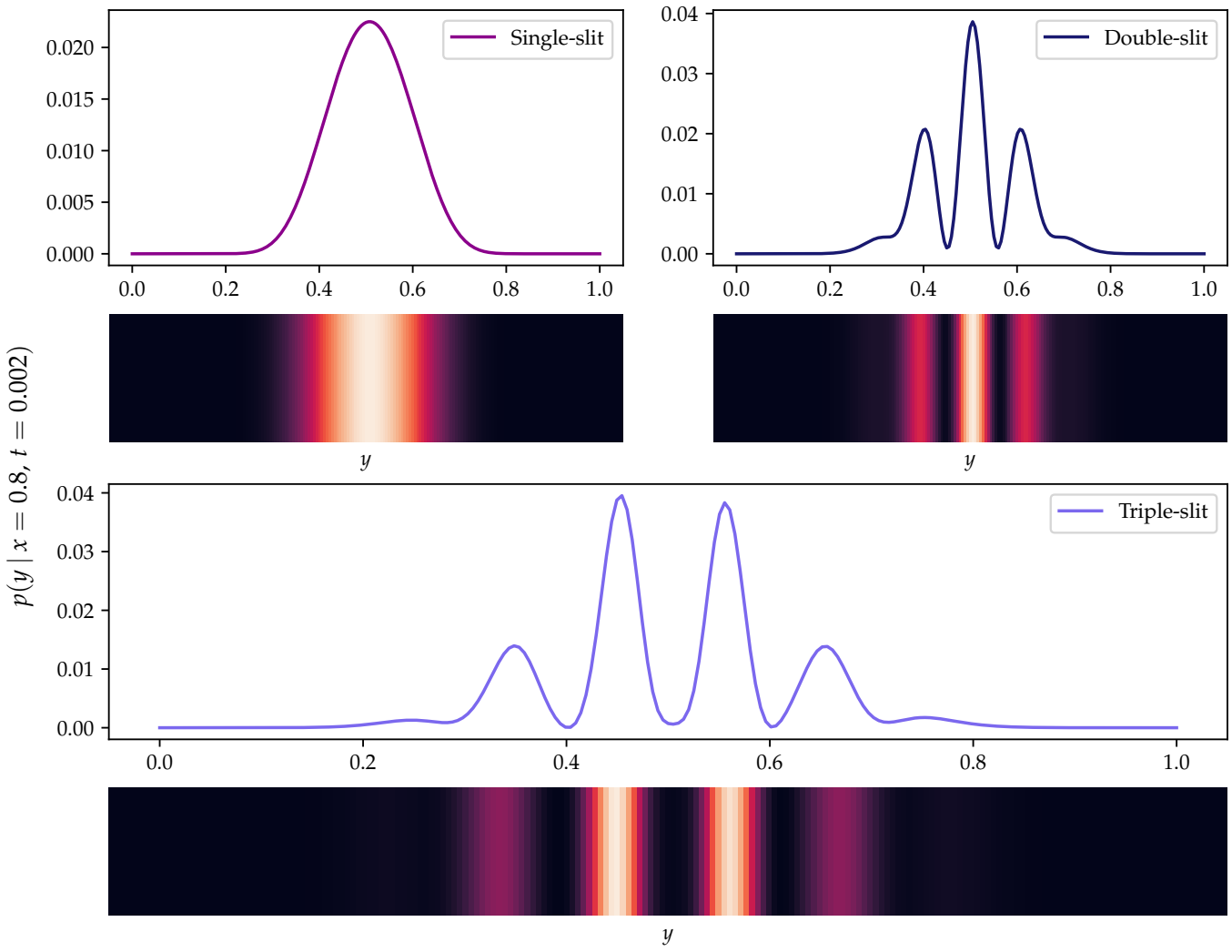

FIG. 5. A figure showing the detection probability $p(y|x = 0.8, t = 0.002)$ for three different configurations: single-slit, double-slit and triple-slit. Each configuration is represented by a line plot of the probability density function above a corresponding heat map. The parameters used for all three heat maps are $h = 0.005$, $\Delta t = 2.5 \cdot 10^{-5}$, $T = 0.002$, $x_c = 0.25$, $\sigma_x = 0.05$, $p_x = 200$, $y_c = 0.5$, $\sigma_y = 0.05$, $p_y = 0$ and $v_0 = 1 \cdot 10^{10}$. All three configurations use a wall thickness of 0.02, positioned at $x = 0.5$ and with slit apertures of 0.05. The distance between the slits of the double and triple-slit configuration is of length $y = 0.05$. The line plots share the same axes, and the one dimensional heat maps share the horizontal axis with the line plots.

IV. DISCUSSION

A. Conservation of the Total Probability

The total probability of the probability function should be conserved over time. This means that we do not let the wave-particle leave the confinements of our experiment. We can use this fact to get an impression of the accuracy concerning the stability of our simulation over time. This is done by plotting the deviation of the total probability from 1.0 for each time step n and see if it stays close to zero. In figure 2 we show the results when calculating the deviation at each time step for a setup with no barrier and a double-slit barrier. We observe that the order of magnitude of the deviation is -15. We use 64-bit floats to represent the numbers in our simulation, this allows us a precision of order -16. Therefore, we can be satisfied with the level of accuracy displayed in the figure. Our choice of method to solve equation 7 - LU Decomposition - is deemed valid when considering the result discussed above.

Another aspect of figure 2 is that the deviation appears to increase. The behaviour is expected and we presume that the level of accuracy continues to decline over time. However, we are only interested in simulating the experiment for short periods of time ($t \in [0, 0.015]$). After all, the interesting behaviour happens when the probability is not evenly distributed.

B. Interaction With a Double-slit Barrier

Figure 3 visualizes the probability $p^n_{i,j}$, as well as the real and imaginary part of the discretized wave function $u^n_{i,j}$ for three different time steps. The first column shows the initial state of the probability cloud at $t = 0$, the second column illustrates the impact as it collides with the barrier and lastly the third column shows it shortly after the impact.

The motion of the probability cloud is governed by the Schrödinger equation, which is a complex valued PDE. When solving the PDE we get a complex valued function that we refer to as the wave function $u^n_{i,j}$. We observe ripples in both the real and imaginary part of $u^n_{i,j}$, which shows us why $u^n_{i,j}$ is referred to as a wave function. This is most clear in the third column at $t = 0.002$.

We have chosen the initial state $u^0_{i,j}$ using a Gaussian wave packet given in equation 10. If we write out the imaginary and real part of the wave packet according to Euler's formula we see that the two parts naturally complement each other. Hence, the ripples are no longer present when the two are combined. We observe the same property for the other time steps as well. Therefore it seems like this property is conserved over time and the probability appears smooth, without any ripples.

When looking at the plots for the time $t = 0.001$, we observe how the probability cloud interacts with a slit-barrier. We show this for single, double and triple-slit configuration in figure 4. We can clearly observe that the probability cloud splits up into multiple parts, where some go through the different slits, and some bounce back. It is further shown in the last column how much the probability cloud has split up and spread out across the room. This visualization is a good way for us to understand how difficult it can be to predict the position of a quantum particle.

C. Interference Pattern

In figure 5, we show the resulting detection probability after measuring the particle using a detector screen. We place the detector screen at $x = 0.8$ so that it spans the entire y-axis at the time $t = 0.002$. We repeat the experiment three times for three different slit configurations. Each configuration is represented as a line plot with a corresponding heat map beneath. The top left of the figure shows the detection probability of when there is a single-slit barrier, the top right of the figure shows a double-slit barrier and the bottom of the figure displays a triple-slit barrier. We assume that the particle passes through the slits and gets detected by the screen. Therefore, the area beneath the probability density function sums to one.

We see an interference pattern emerge as we move from one slit to multiple slits in figure 5. For the single-slit we see what appears to be a Gaussian distribution, evenly spread out around the placement of the slit at the position $y = 0.5$. This is as expected, since we do not anticipate an interference pattern to emerge from a single wave. When we use two slits, however, an interference pattern emerges. This is caused as the waves emerging from the two slits interfere with each other. Since the wave packet hits the two slits symmetrically and concurrently, it evenly distributes into two parts in phase with each other. Therefore, we observe a symmetrical and clear interference pattern with the largest peak at the centre of the detector. As for the case where there are three slits in the barrier, we get two large peaks around the centre instead of one. These interference patterns are not too different to what Thomas Young showed in his original experiment [1]. In the same way as his experiment showed the wave-like behaviour of light, we have demonstrated how the Schrödinger equation gives rise to an interference pattern.

V. CONCLUSION

We have used a dimensionless version of the Schrödinger equation to simulate the probability cloud of a single non-relativistic particle when interacting with three different slit configurations. First, we discretized the Schrödinger equation according to the Crank-Nicolson approach. Then we used a Gaussian wave packet to initialize our wave function $u^0_{i,j}$, and con-

structed the potential matrix V so that it could have a barrier with a single-, double- or triple-slit configuration. Our following strategy was to numerically compute the Crank-Nicolson discretization with an LU decomposition, i.e. solving $Au_{i,j}^{n+1} = Bu_{i,j}^{n}$ with $A = LU$ using the C++ library armadillo. The strategy resulted in a stable conservation of the total probability. We then animated the interaction behavior of the probability cloud for single-, double- and triple-slits over the time $t = 0$ to $t = 0.015$. For the animation we used the square root of the probability so we could observe the highly unlikely probabilities as well. We also visualized the real and imaginary parts of u, which showed clear ripple-like visuals and illustrated why it is referred to as a wave function. Lastly, we made a plot of the interference pattern that occurs for the three different slit configurations. We presented this as a line plot of the probability density with a corresponding heat map. The figures and animations gave a clear visualization of how a non-relativistic particle behave and the interference pattern that emerges in the double-slit experiment.

VI. CODE

The code used to simulate the experiment is available at this Github repository.

Appendix A: Numerical Notation

We use the discretized notations

$$x \to x_i = ih, \qquad i = 0, 1, .., M-1 \tag{A1}$$
$$y \to y_j = jh, \qquad j = 0, 1, .., M-1 \tag{A2}$$
$$t \to t_n = n\Delta t, \qquad n = 0, 1, .., N_t - 1. \tag{A3}$$

$$u(x, y, t) \to u(ih, jh, n\Delta t) \equiv u_{i,j}^{n}, \tag{A4}$$
$$v(x, y) \to v(ih, jh) \equiv v_{i,j}, \tag{A5}$$

where $x \in [0, 1], y \in [0, 1], t \in [0, T]$. The vector $\vec{u}^n$ is a column vector that contains the values $u_{i,j}^n$ as follows:

$$\vec{u}^{\,n} = \Big[(u_{1,1}^n, u_{2,1}^n, .., u_{M-2,1}^n), (u_{1,2}^n, u_{2,2}^n, .., u_{M-2,2}^n), \ldots, (u_{1,M-2}^n, u_{2,M-2}^n, .., u_{M-2,M-2}^n)\Big]. \tag{A6}$$

Appendix B: Analytical

$$\frac{\partial^2 u}{\partial x} = \frac{u_{i+1,j}^n - 2u_{i,j}^n + u_{i-1,j}^n}{h^2}. \tag{B1}$$

$$\frac{\partial^2 u}{\partial y} = \frac{u_{i,j+1}^n - 2u_{i,j}^n + u_{i,j-1}^n}{h^2}. \tag{B2}$$

$$u(x = 0, y, t) = 0 \tag{B3}$$
$$u(x = 1, y, t) = 0 \tag{B4}$$
$$u(x, y = 0, t) = 0 \tag{B5}$$
$$u(x, y = 1, t) = 0 \tag{B6}$$

$$A = \begin{bmatrix} a_0 & -r & 0 & -r & 0 & 0 & 0 & 0 & 0 \\ -r & a_1 & -r & 0 & -r & 0 & 0 & 0 & 0 \\ 0 & -r & a_2 & 0 & 0 & -r & 0 & 0 & 0 \\ -r & 0 & 0 & a_3 & -r & 0 & -r & 0 & 0 \\ 0 & -r & 0 & -r & a_4 & -r & 0 & -r & 0 \\ 0 & 0 & -r & 0 & -r & a_5 & 0 & 0 & -r \\ 0 & 0 & 0 & -r & 0 & 0 & a_6 & -r & 0 \\ 0 & 0 & 0 & 0 & -r & 0 & -r & a_7 & -r \\ 0 & 0 & 0 & 0 & 0 & -r & 0 & -r & a_8 \end{bmatrix} \tag{B7}$$

$$B = \begin{bmatrix} b_0 & r & 0 & r & 0 & 0 & 0 & 0 & 0 \\ r & b_1 & r & 0 & r & 0 & 0 & 0 & 0 \\ 0 & r & b_2 & 0 & 0 & r & 0 & 0 & 0 \\ r & 0 & 0 & b_3 & r & 0 & r & 0 & 0 \\ 0 & r & 0 & r & b_4 & r & 0 & r & 0 \\ 0 & 0 & r & 0 & r & b_5 & 0 & 0 & r \\ 0 & 0 & 0 & r & 0 & 0 & b_6 & r & 0 \\ 0 & 0 & 0 & 0 & r & 0 & r & b_7 & r \\ 0 & 0 & 0 & 0 & 0 & r & 0 & r & b_8 \end{bmatrix} \tag{B8}$$

[1] E. Tretkoff, May 1801: Thomas young and the nature of light (2008), (accessed: 14.12.2021).

[2] J. E. Baggott, Wave mechanics, in *The meaning of quantum theory: A guide for students of chemistry and physics* (Oxford University Press, 1993) pp. 20–21, (accessed: 12.12.2021).

[3] N. P. Landsman, Born rule and its interpretation, in *Compendium of Quantum Physics*, edited by D. Greenberger, K. Hentschel, and F. Weinert (Springer Berlin Heidelberg, Berlin, Heidelberg, 2009) pp. 64–70, (accessed: 13.12.2021).

[4] C. Sanderson, Armadillo c++ linear algebra library (2016), (accessed: 14.12.2021).